BULLETIN OF THE POLISH ACADEMY OF SCIENCES
TECHNICAL SCIENCES, Vol. 69(1), 2021, Article number: e135835
DOI: 10.24425/bpasts.2021.135835

Optimization of tribology parameters of AZ91D magnesium alloy in dry sliding condition using response surface methodology and genetic algorithm

M. BENIYEL[1]*, M. SIVAPRAGASH[2], S.C. VETTIVEL[3], P. SENTHIL KUMAR[4], K.K. AJITH KUMAR[5], and K. NIRANJAN[6]

[1] Department of Mechanical Engineering, Anna University, Chennai, Tamil Nadu, India
[2] Department of Mechanical Engineering, Universal College of Engineering and Technology, Vallioor, Tirunelveli, Tamilnadu, India
[3] Department of Mechanical Engineering, Chandigarh College of Engineering and Technology, Chandigarh, India
[4] Department of Mechanical Engineering, MET Engineering College, Tamilnadu, India
[5] Department of Mechanical Engineering, Rohini College of Engineering and Technology, Tamilnadu, India
[6] Department of Manufacturing Engg, Annamalai University, Annamalai Nagar-608 002, Tamilnadu, India

Abstract. In the present research, the wear behaviour of magnesium alloy (MA) AZ91D is studied and optimized. MA AZ91D is casted using a die-casting method. The tribology experiments are tested using pin-on-disc tribometer. The input parameters are sliding velocity (1–3 m/s), load (1–5 kg), and distance (0.5–1.5 km). The worn surfaces are characterized by a scanning electron microscope (SEM) with energy dispersive spectroscopy (EDS). The response surface method (RSM) is used for modelling and optimising wear parameters. This quadratic equation and RSM-optimized parameters are used in genetic algorithm (GA). The GA is used to search for the optimum values which give the minimum wear rate and lower coefficient of friction. The developed equations are compared with the experimental values to determine the accuracy of the prediction.

Key words: magnesium alloy; pin-on-disc; tribology; dry condition; optimization; casting.

1. Introduction

Magnesium alloy (MA) has light weight and high stiffness. MA has good castability, high specific strength, and good creep resistance [1]. MA AZ91D has good use in a wide range of applications in factories [2]. It is utilized in automobile sectors and has structural applications due to its light weight [3]. MA weighs 33% less than aluminum (Al), 61% less than titanium (Ti), and 77% less than stainless steel (SS). MA is a promising material as a better replacement for the above materials [4].

However, MA is not a good replacement in terms of wear application when it is in contact or it slides with other materials [5]. It has poor temperature stability, poor tribology properties, high susceptibility to thermal expansion, inadequate properties at higher temperatures and it is subject to corrosion [6]. At room temperature condition, MA possible application is now restricted, due to its poor wear resistance properties [7]. MA AZ series are the most common MA, due to their cost, high mechanical strength, and corrosion resistance which were acquired by adding aluminum, zinc, and manganese. The optimal structure of the AZ91 alloy appears to be strengthened by exiting the Al-Mg matrix and creating binary atmospheres with Mg and manganese [8]. The AZ91D alloy is widely used in the construction field and structural applications. It contains Al and Zn as major alloying elements. MA is fabricated by die-cast [9]. Hardness and wear resistance are improved by deep cryogenic heat treatment [10]. Oxidation and abrasion were major wear mechanisms at the lowest sliding loads and low sliding speeds. Increasing sliding speed and loads led to a combination of oxidation wear, delamination wear, and adhesion wear. The highest load applied, high sliding speed plastic deformation, and severe plastic deformation were identified [11].

The design of experiments (DoE) is a very precious tool used to optimize different variables, correspondence, and their outputs with minimal variability [12]. DoE is used to reduce the number of tests and to achieve useful variables in research, rather than multiple tests, which are time-consuming and difficult [13]. Response surface methodology (RSM) is a tool to find the best and optimum condition for the same system and different variables. The RSM is a comprehensive method for analyzing and solving problems considering the independent variables in response. The RSM has the advantage to find an optimal solution [14].

A genetic algorithm (GA) is widely used in different research areas for parameter optimization. GA is a search algorithm designed to mimic the principles of biological evolution

*e-mail: beniyel1989@gmail.com

Manuscript submitted 2020-02-18, revised 2020-09-14, initially accepted for publication 2020-10-19, published in February 2021

in a natural genetic system, which is also known as a stochastic sampling method, and critical or difficult problems are solved in terms of objective functions [15]. The GA model is an easy tool to find out optimal solutions with multi-objective function. It is highly recommended for optimization due to its power, simplicity, and higher efficiency. A GA consists of three major operations to get the optimum result, namely: reproduction, crossover, and mutation [16]. It is a prolific method for solving linear and non-linear problems, promoted by the process of natural selection and genetic evaluation [17].

Even though a lot of literature is available on the tribological study of MA, none of the studies has the effect of tribological parameters of AZ91D MA in dry sliding conditions and optimization. The present research focused on the optimization of the MA AZ91D tribology properties under dry sliding conditions, and the different parameters which affect the tribological properties are sliding velocity, load, and distance. The tribology properties are optimized and the optimized model results with the RSM and GA validated.

2. Experimental methods

2.1. Materials. MA AZ91D was fabricated using the gravity die casting method. The muffle furnace was initially heated with pure Mg ingots to 750°C [18]. The composition of AZ91D is given in Table 1. Mg ingots were purchased from Kastwel Foundries and other elements were purchased from Parshwamani Metals.

Table 1
MA AZ91D chemical composition

Chemical composition of die-cast Mg-alloys								
El	*Al*	*Zn*	*Mn*	*Fe*	*Cu*	*Ni*	*Si*	*Mg*
%	9.10	0.64	0.17	0.001	0.001	0.001	0.01	Bal

The other alloying elements of MA AZ91D were preheated and added to the furnace. The metal available in the furnace slowly melted and the argon gas was continuously supplied inside the furnace. Before pouring the molten metal, the die is preheated at 250°C for eliminating casting defects. The testing specimens were sliced from the AZ91D MA die-cast ingot and machined to the required shape and different dimensions. The testing specimens were polished by using 600, 800, 1000, and 1200 grit papers and cleaned by acetone solution.

2.2. Wear test. A tribometer (Ducom pin-on-disc tribometer) was utilized to perform dry sliding wear tests on MA AZ91D specimens using the pin-on-disc configuration. The specimen whose size is 10 mm in diameter with a 20-mm height of pin, the track diameter is 100 mm. EN31 steel was used as the counter-face disc (with a diameter of 165 mm and 8 mm thick plate). The wear test specimen was prepared according to the ASTM G99 standard. The specimens were properly cleaned with acetone solution using an ultrasonicator for 10 min before the tribological tests. The tribological tests were performed at various sliding speed of 1, 2, 3 m/s, a various load of 1, 3, 5 kg, and various sliding distance of 0.5, 1, 1.5 km at room temperature (25°C). After every test, the counter-face discs were cleaned with acetone to remove the wear debris and traces. The wear specimen pins were weighed before and after each test run using an analytical weighing machine (a resolution of 0.01 mg). The wear loss of the specimens was measured based on the variation in volumetric losses per unit according to a sliding distance before and after the sliding tests. Friction force was continuously recorded by a load cell in order to evaluate the coefficient of friction (CoF). Each test was repeated three times to ensure repeatability in the friction and wear and their average was reported.

2.3. Optimization.

2.3.1. Response surface methodology. The tribology input parameters for pin-on-disc in dry conditions were optimized. The RSM experimental design was developed based on 3 levels and 3 factors of Box-Behnken design methods [19]. The uncoded values are used in this optimization. The variable levels are middle level (0) which represents the centre point and the batches of every variable at a lower level (–1) or higher level (+1) include verifying of Design Expert 19 or Minitab 19.

2.3.2. Genetic algorithm. A GA was developed by Matlab 2018. It was used to predict the minimum wear rate and CoF within the range of the input parameters. The parameters are sliding velocity (1 to 3 m/s), load (1 to 5 kg), and distance (0.5 to 1.5 km). The optimal variable was validated by using a GA. The percentages of errors were compared to the GA predicted against experimental values, and the accuracy of the prediction was checked and compared.

3. Results and discussion

3.1. Mathematical model using RSM. RSM was used to predict the impact of independent test factors and their correlation for minimum wear rate and minimum CoF with different input parameters. Considering quadratic terms, linear terms, and all interactions, the second-order RSM model is chosen to fit the response surface, and the general shape of the model is described in Eqs. (1) and (2)

$$Y = N_0 + \sum_{i=1}^{n} N_i x_i + \sum_{i=1}^{n} N_{ii} x_i^2 + \\ + \sum\sum_{i<j} N_{ij} x_i x_j + \varepsilon \quad (1)$$

where Y represents the estimated response; N_0 is the constant item; N_i represents the primary coefficient of the independent variable x_i; N_{ij} is the correlation coefficient between the independent variables x_i, x_j; and Nii represents the quadratic coefficient associated with the independent variable x_i [20]. The

second-order polynomial quadratic regression equation is given in Eq. (2)

$$Y = \beta 0 + \beta 1V1 + \beta 2V2 + \beta 3V3 + \beta 11V1^2 + \\ + \beta 22V2^2 + \beta 33V3^2 + \beta 12V1V2 + \\ + \beta 23V2V3 + \beta 13V1V3 \quad (2)$$

where Y is the dependent variable (wear rate, $mm^3/kg.km$ and CoF); V_1, V_2, V_3 denote the independent variables, viz, sliding velocity (m/s) load (kg), and sliding distance (km). The parameters effects and their interactions in response were analysed by conducting optimal tests and using variance analysis (ANOVA) [21].

Table 2
The levels of input variables

Factors	Uncoded value		
	–1	0	+1
Sliding Velocity (m/s)	1	2	3
Load (kg)	1	3	5
Distance (km)	0.5	1	1.5

3.1.1. Modelling and prediction using RSM. The developed mathematical equations are listed in Eqs. (3) and (4):

$$WR = 6.11 - 2.245\ SV + 1.426\ L - 8.02\ D - \\ - 0.531\ SV * SV - 0.3187\ L * L + \\ + 2.953\ D * D + 0.4480\ SV * L + \\ + 2.868\ SV * D + 0.034\ L * D \quad (3)$$

$$Cof = 0.986 - 0.320\ SV - 0.2285\ L - 0.370\ D + \\ + 0.0527\ SV * SV + 0.03541\ L * L + \\ + 0.0197\ D * D - 0.01400\ SV * L + \\ + 0.1539\ SV * D + 0.0237\ L * D \quad (4)$$

Table 3
Factors and responses

Sl. No	Factors			Actual Factors			Response	
	X1	X2	X3	SV (m/s)	L (kg)	D (km)	WR (mm^3/kg.km)	CoF
1	0	0	0	2	3	1	4.372	0.136
2	0	–1	–1	2	1	0.5	1.235	0.327
3	0	–1	1	2	1	1.5	4.589	0.289
4	–1	1	0	1	5	1	2.53	0.280
5	–1	0	–1	1	3	0.5	4.305	0.243
6	1	0	1	3	3	0.5	0.987	0.084
7	1	0	–1	3	3	0.5	0.957	0.068
8	–1	–1	0	1	1	1	2.608	0.335
9	0	1	–1	2	5	0.5	3.005	0.228
10	0	0	0	2	3	1	4.378	0.140
11	0	0	0	2	3	1	4.352	0.131
12	1	–1	0	3	1	1	0.801	0.436
13	–1	0	1	1	3	1.5	5.459	0.176
14	1	1	0	3	5	1	4.307	0.269
15	0	1	1	2	5	1.5	6.495	0.285

3.2. Effect of parameters on wear rate.

3.2.1. Effects of sliding velocity, load-on-wear rate. An estimate of the interaction between the dimensional response surface plots and the explanatory variables in the properties of the wear is shown. The surface plot shown in Fig. 1a is the effect of sliding velocity vs load concerning various sliding distances, as regards the distance for 0.5 km when the sliding velocity increases (1 to 3 m/s), the wear rate decreases gradually. The load increases (1 to 5 kg) the wear rate increases. The minimum wear rate is observed at high sliding velocity (1 m/s) and low load (1 kg). The maximum wear rate is observed at low sliding velocity (1m/s) and high load at (5 kg). The surface plot in Fig. 1b shows the distance of 1 km. When the sliding velocity increases (1 to 3 m/s), the wear rate is decreased gradually. The load is increased (1 to 5 kg) as the wear rate increases. The minimum wear rate is observed at high sliding velocity (3 m/s) and low load (1 kg) condition. The maximum wear rate is observed at high sliding speed (3m/s) and high load (5 kg)

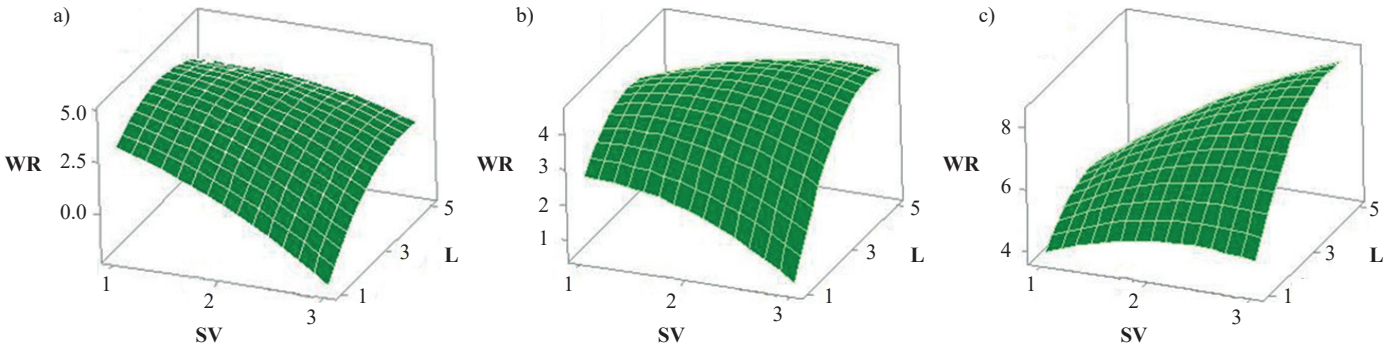

Fig. 1. Surface plots between sliding velocity vs load-on-wear rate (WR), with respect to various distances: a) D – 0.5; b) D – 1.0; c) D – 1.5 km

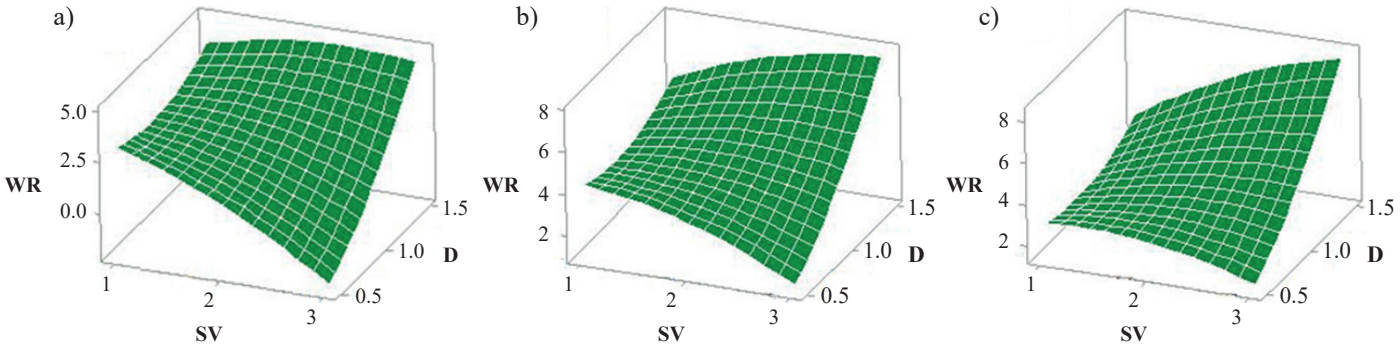

Fig. 2. Surface plots of sliding velocity vs distance-on-wear rate, with respect to various loads: a) L – 1; b) L – 3; c) L – 5 kg

condition. The surface plot shown in Fig. 1c shows the distance of 1.5 km. The sliding velocity increases (1 to 3 m/s), the wear rate increases gradually. The load is increased (1 to 5 kg) as the wear rate increases. The minimum wear rate is observed at low sliding velocity (1 m/s) and low load (1 kg) condition. The maximum wear rate is observed at high sliding velocity (3 m/s) and high load (5 kg) conditions.

3.2.2. Effect of sliding velocity (SV), distance (D) and wear rate (WR). The surface plot when developed helps to understand the relations between interaction variables easily [22]. The optimized sample could expand our understanding [23]. The surface plot in Fig. 2a shows the effect of sliding velocity, distance, and load for 1 kg. When the sliding velocity increases (1 to 3 m/s), the wear rate decreases gradually. When the distance is increased (0.5 to 1.5 km), the wear rate increases. The minimum wear rate is observed at high sliding velocity (3 m/s) and low distance (0.5 km). The maximum wear rate is observed at high sliding velocity (3 m/s) and high distance (1.5 km) condition. The surface plot in Fig. 2b shows the load of 3 kg. When the sliding velocity increases (1 to 3 m/s), the wear rate decreases gradually. At the distance increases (0.5 to 1.5 km) the wear rate also increases. The minimum wear rate is observed at high sliding velocity (3 m/s) and low distance (0.5 km) conditions. The maximum wear rate is observed at high sliding velocity (3 m/s) and high distance (1.5 km) conditions. The surface plot in Fig. 2c shows the load for 5 kg. When the sliding velocity increases (1 to 3 m/s), the wear rate decreases gradually. When the distance is increased (0.5 to 1.5 km), the wear rate also increases. The minimum wear rate is observed at high sliding velocity (3 m/s) and low distance (0.5 km) conditions. The maximum wear rate is observed at high sliding velocity (3 m/s) and high distance (1.5 km) conditions.

3.2.3. Effect of load (L), distance (D) and wear rate (WR). The surface plot in Fig. 3a shows the effect of load, distance, and sliding velocity of 1 m/s. When the load is increased (1 to 3 kg), the wear rate is also increased. When the load is further increased (3 to 5 kg), the wear rate decreases. When the distance is increased (0.5 to 1 km), the wear rate is decreased. The wear rate is increased at a distance (1 to 1.5 km). The minimum wear rate is observed at a high load (5 kg) and mid-distance (1 km). The maximum wear rate is observed at mid-load (3 kg) and high distance (1.5 km) conditions. The surface plot in Fig. 3b shows the sliding velocity of 2 m/s. When the load is increased (1 to 3 kg), the wear rate is also increased. The wear rate is slightly decreased when the load is increased (3 to 5kg). The distance is increased at (0.5 to 1.5 km) and the wear rate is increased. The minimum wear rate is observed at low load (1 kg) and low distance (0.5 km). The maximum wear rate is observed at mid-load (3 kg) and high distance (1.5 km). The surface plot in Fig. 3c shows the sliding velocity of 3 m/s. When the load is increased (1 to 5 kg), the wear rate is increased. When the distance is increased at (0.5 to 1.5 km), the wear rate is also increased. The minimum wear rate is observed at low load (1 kg) and low distance (0.5 km). The maximum wear rate is observed at mid-load (5 kg) and high distance (1.5 km). The optimized parameters and their responses are listed in Tables 2 and 4.

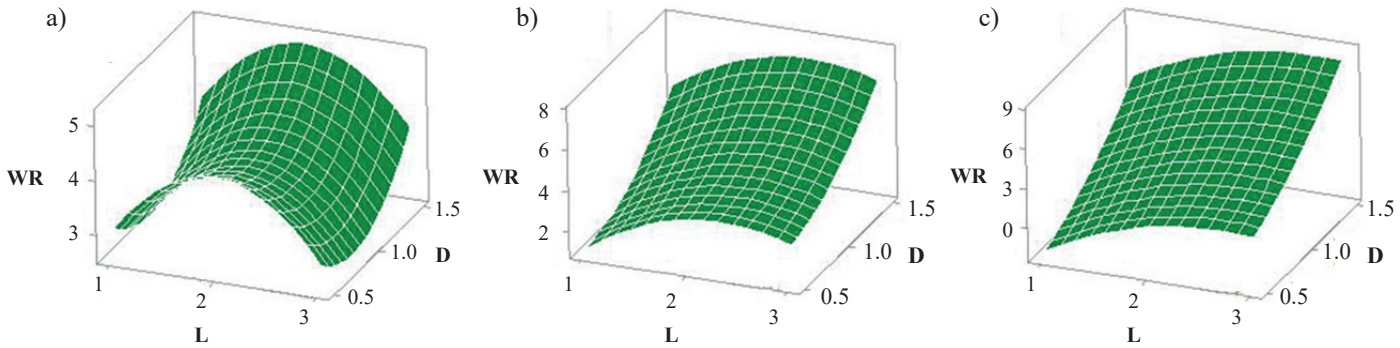

Fig. 3. Surface plots between load vs distance-on-wear rate, with respect to various sliding velocity: a) SV – 1; b) SV – 2; c) SV – 3 m/s

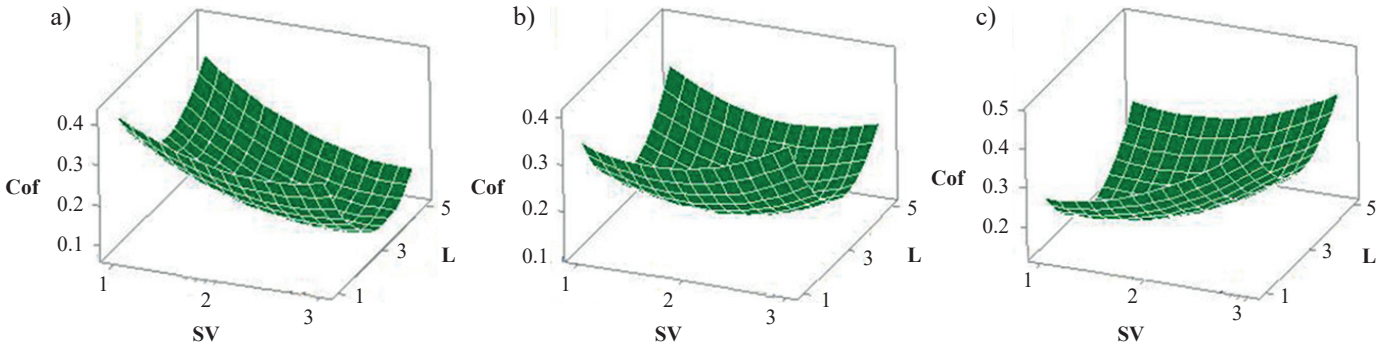

Fig. 4. Surface plots of sliding velocity vs load on CoF with various distances: a) D – 0.5; b) D – 1; c) D – 1.5 km

3.3. Effect of the coefficient of friction.

3.3.1. Effect of sliding velocity, load on CoF. The coefficient of friction is the ratio between the friction and normal force. It is constantly and accurately observed by a load cell in order to evaluate the CoF in the wear slide [24]. The 3-dimensional response surface plots show the evaluation of the interaction between explanatory variables on CoF properties. The surface plot in Fig. 4a shows the effect of sliding velocity, load, and distance for 0.5 km. The CoF decreases while increasing the sliding velocity (1 to 3 m/s). When the load is increased (1 to 3 kg), the CoF is decreased, and load is increased (3to 5 kg), the CoF is increased. The minimum CoF value is observed at high sliding velocity (3 m/s) and mid load (3 kg). The maximum CoF observed at a low sliding speed (1 m/s) and low load (1 kg). The surface plot in Fig. 4b shows the distance of 1 km. The CoF increases while increasing the sliding velocity (1 to 3 m/s). When the load increases (1 to 3 kg), the CoF decreases. The CoF increases as the load increases (3 to 5kg). The minimum CoF is observed at low sliding velocity (1 m/s) and mid load at (3 kg). The maximum CoF is observed at high sliding velocity (3 m/s) and low load (1 kg) conditions. The surface plot in Fig. 4c shows the distance of 1.5 km. The CoF increases while increasing the sliding velocity (1 to 3 m/s). When the load is increased (1 to 3 kg), the CoF is decreased. The CoF is increased as load increases (3 to 5 kg). The minimum CoF value is observed at low sliding velocity (1 m/s) and mid load (3 kg). The maximum CoF is observed at high sliding velocity (3 m/s) and low load (1 kg).

3.3.2. Effect of sliding velocity, distance on CoF. The surface plot in Fig. 5a shows the effect of sliding velocity, distance, and load for 1 kg. The CoF is decreased when the sliding velocity increases (1 to 3 m/s). When the distance increases (0.5 to 1.5 km), the CoF increases gradually. The minimum CoF is found at low sliding velocity (1 m/s) and high distance (1.5 km). The maximum CoF is observed at high sliding velocity (3 m/s) and high distance (1.5 km). The surface plot in Fig. 5b shows the load for 3 kg. When the sliding velocity increases (1 to 3 m/s), the CoF decreases gradually. When the distance increases (0.5 to 1.5 km), the CoF increases suddenly. The minimum CoF is observed at high sliding velocity (3 m/s) and low distance (0.5 km). The maximum CoF is observed at high sliding velocity (3 m/s) and high distance (1.5 km). The surface plot in Fig. 5c shows the load for 5 kg. When the sliding velocity increases from 1 m/s to 3 m/s, the CoF decreases suddenly. When the distance increases from 0.5 to 1.5 km, the CoF increases suddenly. The minimum CoF is observed at a high sliding velocity of 3 m/s and a low distance of 0.5 km. The maximum CoF is observed at a high sliding velocity of 3 m/s and a high distance of 1.5 km.

3.3.3. Effect of load, distance on CoF. The surface plot in Fig. 6a shows the effect of load, distance, and sliding velocity of 1 m/s. The CoF is decreased at a load (1 to 3 kg) and low distance (0.5 km). The CoF is slightly increased, when the load increases (3 to 5 kg) and low distance (0.5 km). The CoF decreases as distance increases (0.5 to 1.5 km). The lowest CoF

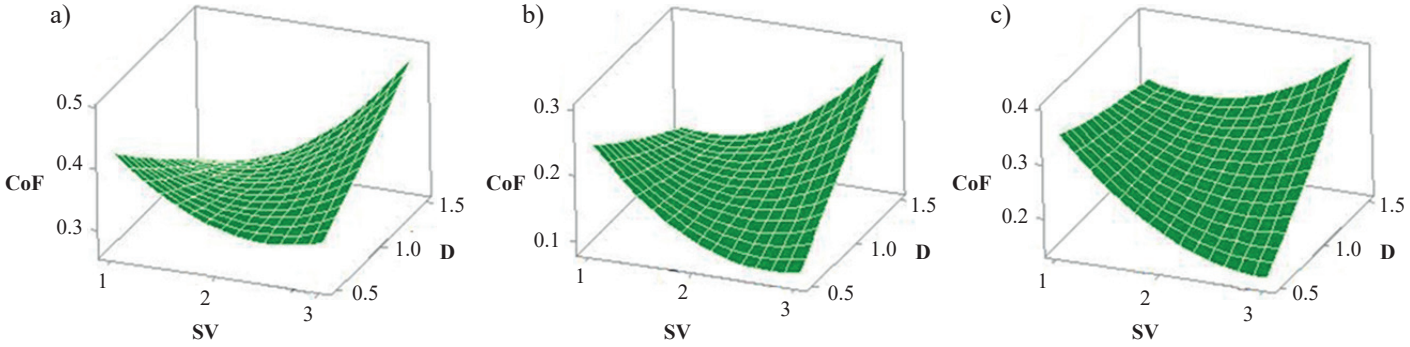

Fig. 5. Surface plots of sliding velocity vs distance on CoF with various loads: a) L – 1; b) L – 3; c) L – 5 kg

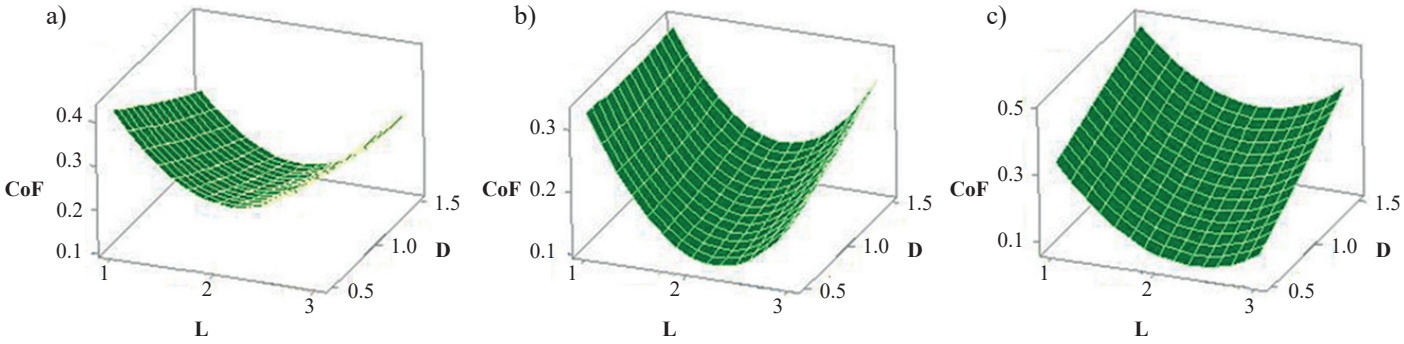

Fig. 6. Surface plots of load vs distance on CoF with various sliding velocities: a) SV – 1; b) SV – 2; c) SV – 3 m/s

is observed at a mid-load (3 kg) and high distance (1.5 km). The maximum CoF is observed at a low load (1 kg) and low distance (0.5 km). The surface plot in Fig. 6b shows the sliding velocity of 2 m/s. The CoF value is dropped suddenly at load (1 to 3 kg) and low distance (0.5 km). The CoF is increased while the load increases (3 to 5 kg) and at a low distance (0.5 km). The CoF increases as distance increases (0.5 to 1.5 km). The lowest CoF is observed at mid-load (3 kg) and low distance (0.5 km). The maximum CoF observed at low load (1 kg) and low distance (0.5 km). The surface plot in Fig. 6c shows the sliding velocity of 3 m/s. The CoF value is dropped gradually at load (1 to 3 kg) and low distance (0.5 km). The CoF is increased while load increases (3 to 5 kg) and low distance (0.5 km). The CoF increases as distance increases (0.5 to 1.5 km). The lowest CoF is observed at mid-load (3 kg) and low distance (0.5 km). The maximum CoF observed at low load (1 kg) and low distance (1.5 km).

3.4. RSM optimization. The optimized parameter's condition is tested using pin-on-disc apparatus. The wear rate and CoF are measured in the testing period. The test results are calculated and compared with the wear rate and CoF is predicted.

Table 4
Optimized parameters using RSM

Sl. No	Parameters	Value
1	Siding Velocity (m/s)	3.0
2	Load (kg)	2.818
3	Distance (km)	0.5

The RSM optimized condition values are sliding velocity is 3 m/s, load 2.818 kg and distance 0.5 km as shown in Table 4. The optimized condition test results are compared with the predicted RSM result. The optimized experimental condition wear rate is 0.9529 (mm^3/kg.km) and the CoF is 0.1046. The optimized condition wear rate is 0.05% of error and the CoF gets 0.28% of error shown in Table 9.

3.5. Genetic algorithm. The GA Tool in Matlab 2018 was used to predict the lowest wear rate and CoF within the range of input parameters. The optimization was designed using standard mathematical design with the empirical quadratic mathematical model. The optimization and associated test validation are shown in Table 4. This is observed from the table. The test results match GA predictions (less than 5% error in the prediction). GA was used to search for optimal values, which yielded the lowest wear rate and lowest the CoF. The parameters (5a, 5b, 5c) are selected for GA to check the predicted optimal values. Three tests were performed using the same condition predicted by GA. The average values obtained were compared with the predicted values to determine the accuracy of the prediction [25]. The objective equation is shown in Eq. (5).

3.5.1. Genetic algorithm optimization. The purpose of the optimization process in this study is to find the optimal input parameter conditions were led to the minimum value of the wear rate and the minimum CoF. The mathematical model proposed in Eqs. (3) and (4) is taken to define the objective function and is expressed as follows. The wear rate and CoF are minimised.

$$\begin{aligned} Eq = {} & 6.11 - 2.245\,SV + 1.426\,L - 8.02\,D - \\ & - 0.531\,SV * SV - 0.3187\,L * L + \\ & + 2.953\,D * D + 0.4480\,SV * L + \\ & + 2.868\,SV * D + 0.034\,L * D - 0.986 + \\ & + 0.320\,SV + 0.2285\,L + 0.370\,D - \\ & - 0.0527\,SV * SV - 0.03541\,L * L - \\ & - 0.0197\,D * D + 0.01400\,SV * L - \\ & - 0.1539\,SV * D - 0.0237\,L * D \end{aligned} \tag{5}$$

Subtracting the objective function value of Eq. (5) is subject to limitations. The minimum and maximum limits of the test design are used to define the listed below for GA optimization constraints in Eqs. (5a–5c)

$$1\ \text{m/s} \leq SV \leq 3\ \text{m/s} \tag{5a}$$

$$1\ \text{kg} \leq L \leq 5\ \text{kg} \tag{5b}$$

$$0.5\ \text{km} \leq D \leq 1.5\ \text{km} \tag{5c}$$

Table 5
GA parameter for the optimal solution

Parameters	**Data and Function type**
Generations	300
Selection type	tournament selection
Mutation probability	0.05
Reproduction probability	0.85
Selection probability	0.85

Table 6
GA predicted variables and responses

Sl. No	Optimum Variables			Output Response	
	SV	L	D	WR	CoF
1	3.000	1.04	1	0.7044	0.393
2	3.060	1.14	0.99	0.7236	0.382
3	2.999	1.0	1.024	0.7786	0.403
4	2.967	1.0	1.025	0.8500	0.399
5	3.016	1.005	1.002	0.6083	0.401
6	3.020	0.98	1.032	0.7443	0.411
7	2.913	1.112	0.96	0.7861	0.364
8	2.963	1.031	1.002	0.7750	0.390
9	3.001	1.012	1.026	0.8138	0.402
10	3.001	1.0	1.026	0.7878	0.404

Best and average fitness values show a gradual convergence towards the optimum value of 1.0952 after 125 generations show in Fig. 7, which implies that copying an individual according to their fitness functions leads to a favour probability of offering to provide precise offspring in the next generation.

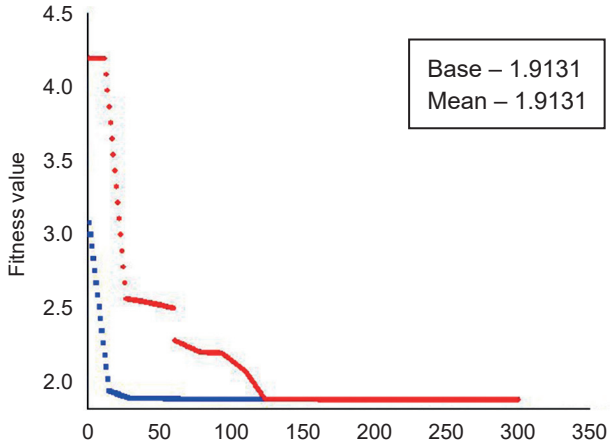

Fig. 7. GA optimise variation of fitness function plot

In a GA, various mutation operators and cross-overs were used to predict the optimized wear rate and CoF conditions. The optimized wear parameters predicted by a GA for obtaining the wear rate and CoF are shown in Table 9. The optimized parameters are shown in Table 7. The GA optimized parameters are sliding velocity (3.016 m/s), load (2.812 kg), and distance (0.515 km).

Table 7
Optimized parameters using GA

Sl. No	**Parameters**	**Values**
1	Sliding velocity (m/s)	3.016
2	Load (kg)	2.812
3	Distance (km)	0.515

The GA response values of the wear rate and CoF are shown in Table 7. The GA optimized response values are compared with the experimental values. The percentage of error is lower, so the GA validation is highly precious.

Table 8
Validation of responses

Wear predict	CoF predict	Wear experiment	CoF experiment	% Error (wear)	% Error (CoF)
0.9554	0.1061	0.9553	0.1062	0.01	0.09

Table 9
Comparison of RSM and GA

Optimization method	WR (Pred)	WR (Exp)	CoF (Pred)	CoF (Exp)	% Error (WR)	% Error (CoF)
RSM	0.9524	0.9529	0.1049	0.1046	0.05	0.28
GA	0.9554	0.9553	0.1061	0.1062	0.01	0.09

This comparison helps to find which optimization method had a high accuracy in the prediction. The RSM and GA optimize processes comparison between predicted versus experiment results. In comparison to the GA, the RSM has a higher error percentage of the wear rate (0.05%), compared to the GA error percentage of the wear rate (0.01%). The RSM CoF error percentage (0.28%) is higher than the GA CoF error percentage (0.09%). From this comparison, the GA optimization has higher accuracy than the RSM optimization method.

3.6. Wear mechanisms. The wear study shows mainly five different wear mechanisms: abrasive wear, oxidation wear, delamination wear, plastic deformation wear, and adhesion wear with less time. The AZ91D MA wear gradually increases while increasing the load and sliding velocity [26]. Based on Archard's equation, the increased hardness enhances the resistance of wear rate and improves the resistance of the materials against plastic deformation [24]. A higher load and higher sliding velocity will make the wear rate high. The lower condition of sliding velocity is 1 m/s, load 1 kg, and distance 0.5 km. The worn surface is shown in Fig. 8, where the plough and grooves are seen on the surface. The hard particles' hardness is higher than the wear specimen, so hard particles make a line on the

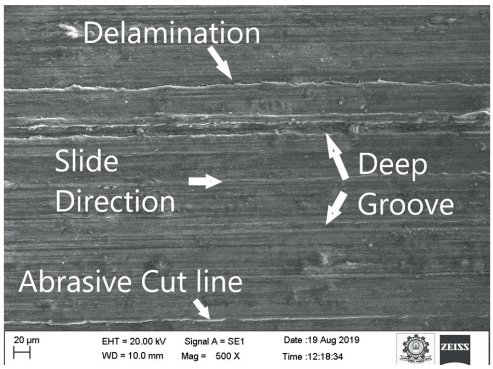

Fig. 8. SEM micrographs at lower condition (sliding velocity 1 m/s, load 1kg and distance 0.5 km)

specimen's surface [5, 27]. The deep grooves in the surface represent abrasive wear [28].

The medium condition of sliding velocity is 2 m/s, load 3 kg, and distance 1 km. The sliding velocity and mid load increased the contact surface. This condition clearly represents the delamination and oxidation wear that occurred on the specimen's surface. The surface of AZ91D MA is slightly removed at the edge of grooves. The extended or removed material flakes from the worn surface is called delamination wear. The oxide particles are present on the worn surface shown in Fig. 9 the removed wear debris metal particles transform oxide due to rise in friction temperature. The oxide particles significantly reduce metal to metal contact. The wear rate is low with the presence of oxide particles and provides better resistance against wear. As per the EDX results shown in Fig. 10 and Table 10, the Oxygen peak shows the 14.5% oxygen content present in the oxidation wear zone. This condition oxidation wear was observed [29].

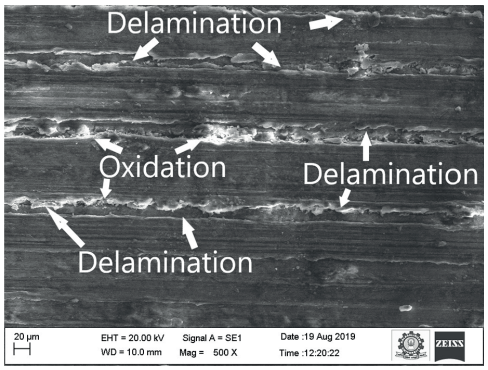

Fig. 9. SEM micrograph at medium condition (sliding velocity 2 m/s, load 3 kg and distance 1 km)

The AZ91D surface is softened by the frictional heat of the revolving disc. The worn surface in Fig. 11 shows that plastic deformation occurred due to a high sliding speed and high load. The metal surface is either softened by the higher frictional temperature of the transport, or the metal surface of specimens is deformed against the rotation direction [27, 29].

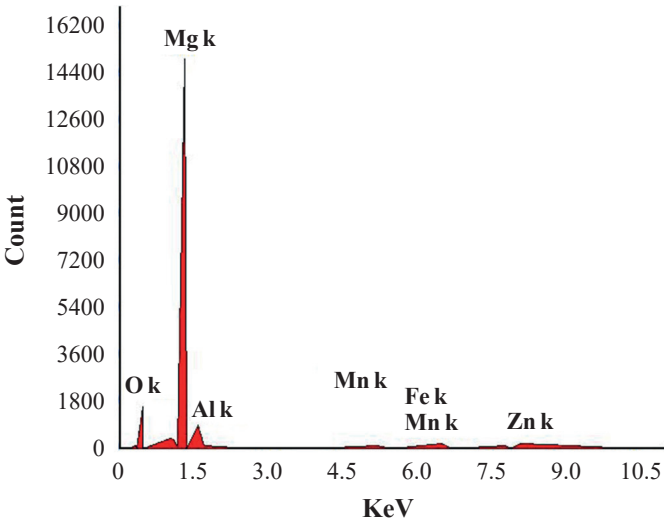

Fig. 10. EDS analysis area surface at SV – 3 m/s, L – 5 kg, and D – 1.5 km and Graphs

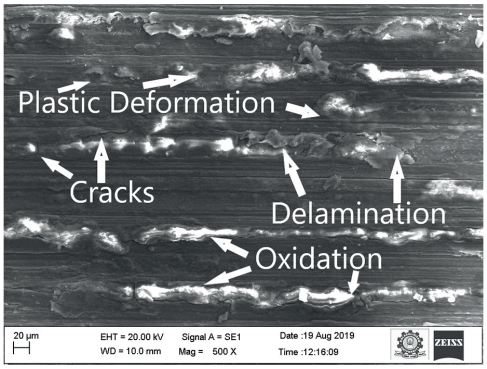

Fig. 11. SEM micrograph of high condition (sliding velocity 3 m/s, load 5 kg, and distance 1.5 km)

The higher condition of sliding speed is 3 m/s, load 5 kg, and distance 1.5 km.

Table 10
EDS identified elements

Elements	Weight %	Atomic %
O	14.5	20.9
Mg	76.2	72.5
Al	6.4	5.5
Mn	0.5	0.2
Fe	0.7	0.3
Zn	1.7	0.6

When the high sliding speed and higher sliding distance is at 3 m/s and 1.5 km, the surface is melted due to a higher temperature developed by friction. The melting point of β-$Mg_{17}Al_{12}$ (437°C) [28].

3.7. Wear surface morphology in optimized conditions. The wear surface of MA AZ91D is analysed in its optimized condition. The optimized parameters are the sliding velocity of 3 m/s, the load of 2.8 kg, and the distance of 0.5 km. These parameters are considered in the validation experiments shown in Table 7. They wear worn surfaces in optimized conditions characterized by SEM in an optimized validated experiment.

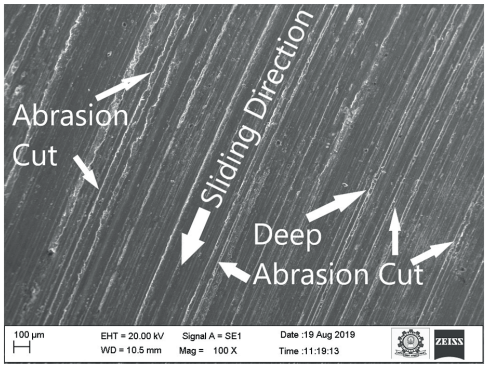

Fig. 12. SEM image at optimized condition (SV – 3 m/s, L – 2.8 kg, and D – 0.5 km)

The load is 2.8 kg, and the sliding velocity is 3 m/s, for a sliding distance of 0.5 km. The removed debris gets oxide easily. The plough and grooves are seen on the surface. The hard particles make line marks on the specimen's surface [5], due to load (Medium), low distance, and high sliding speeds. Deep grooves clearly show on the specimen surface, representing its abrasive wear. The debris act as the hardest abrasive particles and cut the line grooves on the surface of the specimens [27], as shown in Fig. 12. This mechanism is called abrasive wear. The optimized validation experiment clearly shows a lower wear rate. The abrasive wear is only identified in SEM Fig. 12. So, the optimum wear rate occurred in sliding condition parameters at SV – 3 m/s, L – 2.8 kg, and D – 0.5 km. There were no oxidation, delamination, and other wear mechanisms identified in the optimized condition.

4. Conclusions

The MA AZ91D has been cast using the gravity die-casting process without any major defects. Based on the tribological experimental and analysis results, the following conclusions are drawn:

- The wear tests were conducted using the ASTM G99 standard. The tribological parameters were modelled and optimized using RSM Box-Behnken Method.
- The effects of wear rate are higher load made a higher wear rate. Higher distance made higher wear rate. The higher sliding velocity made a low wear rate.
- The effects of CoF mean higher load makes high CoF. High sliding distance made higher CoF. The higher sliding distance made low CoF.
- The optimized values using RSM were sliding velocity 3 m/s, load 2.818 kg, distance 0.5 km and responses wear rate was 0.9529 mm^3/kg.km and CoF 0.1046.
- Optimized values using GA were sliding velocity 3.016 m/s, load 2.812 kg, distance 0.515 km and responses wear rate was 0.9554 mm^3/kg.km and CoF 0.106.
- The developed models had good agreements with experimental and predicted value, and with much fewer errors in GA.
- The MA AZ91D dry condition tribology surface was analysed. The wear mechanisms identified were abrasive, oxidation, delamination, and plastic deformation.
- RSM optimized models were developed for input parameters sliding velocity, load, and distance, for the response of wear rates and coefficient of friction, respectively. The results of ANOVA confirm the prediction models had an adequate approximation to the actual values.
- The interaction effects on the tribology properties of MA AZ91D were investigated using a 3D response surface. The comparison was made between the predicted and actual values using a GA.
- The optimum wear rate and a low CoF were obtained for MA AZ91D. The optimal parameters were SV = 3 m/s, L = 2.8 kg, D = 0.5 km.

References

[1] S. Kulkarni, D. Edwards, E. Parn, C. Chapman, C. Aigbavboa, and R. Cornish, "Evaluation of vehicle light-weighting to reduce greenhouse gas emissions with focus on magnesium substitution", *J. Eng. Design Technol.* 16(6), 869–888 (2018).

[2] K. Kudła, J. Iwaszko, and M. Strzelecka, "Surface modification of AZ91 magnesium alloy using GTAW technology", *Bull. Pol. Ac.: Tech.* 65(6), 917–926 (2017).

[3] K. Soorya Prakash, P. Balasundar, S. Nagaraja, P.M. Gopal, and V. Kavimani, "Mechanical and wear behaviour of Mg–SiC–Gr hybrid composites", *J. Magnes. Alloy.* 4, 197–206 (2016).

[4] D. Mehra, M. Mahapatra, and S. Harsha, "Optimizations of RZ5-TiC magnesium matrix composite wear parameters using Taguchi approach", *Ind. Lubr. Tribol.* 70(5), 907–914 (2018).

[5] E. Ilanaganar and S. Anbuselvan, "Wear mechanisms of AZ31B magnesium alloy during dry sliding condition, *Mater. Today: Proceedings* 5, 628–635 (2018).

[6] E. Suneesh and M. Sivapragash, "Comprehensive studies on processing and characterization of hybrid magnesium composites", *Mater. Manuf. Process.* 33, 1324–1345 (2018).

[7] T. Yue1 and K. Huang, "Laser cladding of Cu0.5NiAlCoCrFeSi high entropy alloy on AZ91D magnesium substrates for improving wear and corrosion resistance", *World J. Eng.* 9(2), 119–124 (2012).

[8] M. Mondet, E. Barraud, S. Lemonnier, J. Guyon, N. Allain, and T. Grosdidier, "Microstructure and mechanical properties of AZ91 magnesium alloy developed by Spark Plasma Sintering", *Acta Mater.* 119, 55–67 (2016).

[9] P.J. Blau and M. Walukas, "Sliding friction and wear of magnesium alloy AZ91D produced by two different methods", *Tribol. Int.* 33, 573–579 (2000).

[10] S.C. Cagan, M. Aci, B.B. Buldum, and C. Aci, "Artificial neural networks in mechanical surface enhancement technique for the prediction of surface roughness and microhardness of magnesium alloy", *Bull. Pol. Ac.: Tech.* 67(4), 729–739 (2019).

[11] S. García-Rodríguez, B. Torres, A. Maroto, A.J. Lopez, E. Otero, and J. Rams, "Dry sliding wear behavior of globular AZ91 magnesium alloy and AZ91/SiCp composites", *Wear* 390–391, 1–10 (2017).

[12] D. Thirumalaikumarasamy, V. Balasubramanian, and S. Sree Sabari, "Prediction and optimization of process variables to maximize the Young's modulus of plasma sprayed alumina coatings on AZ31B magnesium alloy", *J. Magnes. Alloy.* 5, 133–145 (2017).

[13] A., Mohammadzadeha, M. Ramezania, and A.M. Ghaedib, "Synthesis and characterization of Fe2O3–ZnO–ZnFe2O4 / carbon nanocomposite and its application to removal of bromophenol blue dye using ultrasonic assisted method: Optimization by response surface methodology and genetic algorithm", *J. Taiwan Inst. Chem. Eng.* 59, 1–10 (2015).

[14] M. Vakili-Azghandi, A. Fattah-Alhosseini, and M.K. Keshavarz, "Optimizing the electrolyte chemistry parameters of PEO coating on 6061 Al alloy by corrosion rate measurement: Response surface methodology", *Measurement* 124, 252–259 (2018).

[15] A. Ciszkiewicz and G. Milewski, "Ligament-based spine-segment mechanisms", *Bull. Pol. Ac.: Tech.* 66(5), 705–712 (2018).

[16] M. Sivapragash, P. Kumaradhas, B. Stanly Jones Retnam, X. Felix Joseph, and U.T.S. Pillai, "Taguchi based genetic approach for optimizing the PVD process parameter for coating ZrN on AZ91D magnesium alloy", *Mater. Des.* 90. 713–722 (2016).

[17] Y. Li and X. Wang, "Improved dolphin swarm optimization algorithm based on information entropy", *Bull. Pol. Ac.: Tech.* 67(4), 679–685 (2019).

[18] D. Zhang et al., "Effects of minor Sr addition on the microstructure, mechanical properties and creep behavior of high pressure die casting AZ91–0.5RE based alloy", *Mater. Sci. Eng., A* 693, 51–59 (2017).

[19] M. Nouioua et al., "Investigation of the performance of the MQL, dry, and wet turning by response surface methodology (RSM) and artificial neural network (ANN)", *Int. J. Adv. Manuf. Technol.* 93, 2485–2504 (2017).

[20] I.M. Yusri et al., "A review on the application of response surface method and artificial neural network in engine performance and exhaust emissions characteristics in alternative fuel", *Renew. Sust. Energy Rev.* 90. 665–686 (2018).

[21] S. Jacob and R. Banerjee, "Modeling and Optimization of Anaerobic Codigestion of Potato Waste and Aquatic Weed by Response Surface Methodology and Artificial Neural Network coupled Genetic Algorithm", *Bioresour. Technol.* 214, 386-395 (2016).

[22] S. Shanavas and J. Edwin Raja Dhas, "Parametric optimization of friction stir welding parameters of marine grade aluminium alloy using response surface methodology", *Trans. Nonferrous Met. Soc. China* 27, 2334−2344 (2017).

[23] M.N.M. Salleh, M. Ishak, M.M. Quazi, and M.H. Aiman, "Microstructure, mechanical, and failure characteristics of laser-microwelded AZ31B Mg alloy optimized by response surface methodology", *Int. J. Adv. Manuf. Technol.* 99, 985–1001 (2018).

[24] W. Yu, D. Chen, L. Tian, H. Zhao, and X. Wang, "Self-lubricate and anisotropic wear behavior of AZ91D magnesium alloy reinforced with ternary Ti2AlC MAX phases", *J. Mater. Sci. Technol.* 35, 275–284 (2019).

[25] B.O. Ighose et al., "Optimization of biodiesel production from Thevetia peruviana seed oil by adaptive neuro-fuzzy inference system coupled with genetic algorithm and response surface methodology", *Energy Convers. Manage.* 132. 231–240 (2017).

[26] M.E. Turan, Y. Sun, and Y. Akgul, "Mechanical, tribological and corrosion properties of fullerene reinforced magnesium matrix composites fabricated by semi powder metallurgy", *J. Alloys Compd.* 740, 1149–1158 (2018).

[27] C. Dong, J. Sun, Z. Cheng, and Y. Hou, "Preparation and tribological properties of a microemulsion for magnesium alloy warm rolling", *Ind. Lubr. Tribol.* 71(1), 74–82 (2018).

[28] A. Zafari, H.M. Ghasemi, and R. Mahmudi, "Tribological behavior of AZ91D magnesium alloy at elevated temperatures", *Wear* 292–293, 33–40 (2012).

[29] C. Liang, X. Han, T.F. Su, C. Li, and J. An, "Sliding Wear Map for AZ31 Magnesium Alloy", *Tribol. Trans.* 57, 1077–1085 (2014).